Environmental Science & Technology

pubs.acs.org/est

Article

Continuous Characterization of Insoluble Particles in Ice Cores Using the Single-Particle Extinction and Scattering Method

Chantal Zeppenfeld,* Tobias Erhardt, Camilla Marie Jensen, and Hubertus Fischer

Cite This: https://doi.org/10.1021/acs.est.4c07098

Read Online

ACCESS | Metrics & More | Article Recommendations | Supporting Information

ABSTRACT: This study presents the integration of the single-particle extinction and scattering (SPES) method in a continuous flow analysis (CFA) setup. Continuous measurements with the instrument allow for the characterization of water-insoluble particles in ice cores at high resolution with a minimized risk of contamination. The SPES method can be used to investigate particles smaller than 1 μm, which previously could not be detected by instruments typically used in CFA. Moreover, the SPES method provides not only the particle concentration and size distribution but also the effective refractive index. We show that nonabsorbing mineral particles and absorbing particles from both wildfires and fossil fuel burning can be detected with the SPES method in shallow ice cores from North−East Greenland. The concentration record retrieved with SPES correlates well with established methods used in continuous measurements of dust content in ice cores. Year-to-year variations in the number distribution of the diameter are only detectable by stacking annual layers because of the low nonabsorbing particle concentration of late Holocene ice of approximately 6×10^4 mL^{-1}. The median diameter in the bottom 20 m of the EGRIP-S7 core is found to be 0.75 μm (0.72 μm) during the annual maximum (minimum) in dust concentration.

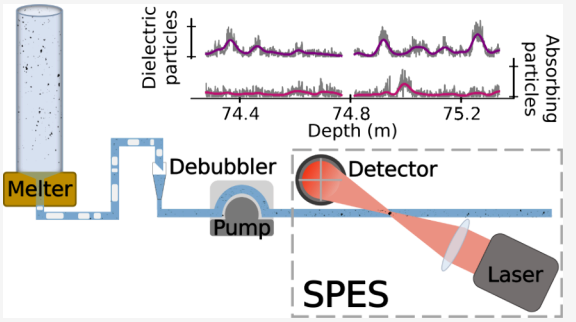

KEYWORDS: *CFA, dust, absorbing particles, ice core, submicron particles*

INTRODUCTION

Ice cores represent archives that contain information about past climatic conditions, such as the composition and aerosol content of the atmosphere. Aerosols, including water-insoluble particles, are deposited on the ice sheets and subsequently preserved in the ice. These particles provide crucial information needed to reconstruct past changes in atmospheric circulation patterns, radiative transfer, and climate conditions in their source regions. Changes in the source regions of the aerosols, transport, and deposition mechanisms are reflected in alterations in the concentration, size distribution, and mineralogy of the particles.[1]

Nonabsorbing, mineral particles found in Greenland ice cores are generally referred to as dust and originate mainly from the Asian deserts (e.g., Taklamakan)[2−4] with additional contribution from other source regions, such as Europe and Africa.[5−8] Absorbing particles are produced during incomplete combustion processes and are of either a biogenic or anthropogenic origin. North America and Siberia are the dominant source regions of the absorbing aerosol black carbon, which is found in ice cores from Greenland.[9−11]

Dust particles affect the biogeochemical cycles, as they provide nutrients to the ocean and land biosphere.[12−14] Furthermore, they scatter and absorb incoming and outgoing radiation, affect the photolysis rates and photochemistry, and act as cloud condensation and ice nuclei.[15−17] Thus, particles impact the Earth's radiative balance. The radiative effect of dust particles is associated with large uncertainties because their size distribution and optical properties are not well constrained.[18,19]

Particle counting and sizing in ice-core analysis is commonly performed with either Coulter counter (CC) instruments, laser-sensing particle detectors (LPDs),[20] or imaging techniques, for example, scanning electron microscopy (SEM).[21,22] Imaging and the CC technique are well-established but only discrete samples can be measured.[23] A continuous measurement technique of water-insoluble particles reduces the risk of contamination and a high-resolution record can be obtained. The Abakus laser sensor, which is an LPD instrument, is commonly used for continuous measurements of ice cores. However, Abakus measurements are restricted to particle sizes larger than 1 μm.

Currently, no continuous concentration or size distribution measurement technique for particles in ice cores smaller than 1 μm exists. The particle size range of 0.1−1 μm is of particular

Received: July 11, 2024
Revised: December 16, 2024
Accepted: December 18, 2024

interest, as it covers the peak of the number size distribution of the accumulation mode. Aerosols in this size range have the longest atmospheric residence time and thus survive long-range transport from their source region to the remote polar ice sheets. Therefore, addressing this research gap is essential for improving the understanding of the processes causing the particle concentration and size distribution changes observed in the ice and for constraining the particle properties in paleoclimate models.

The single-particle extinction and scattering (SPES)[24] method can measure submicron particles continuously but has so far only been applied to discrete ice core measurements.[25,26] The commercially available EOS Classizer One, which uses the SPES method, determines the particle extinction cross section, effective refractive index, and concentration in the size range from 0.2 to 2 μm. This study presents the implementation of the SPES instrument in the Bern continuous flow analysis (CFA) system based on the results of particle measurements from two shallow ice cores from North−East Greenland: ExNGT-B16 and EGRIP-S7.

MATERIALS AND METHODS

Data. The data presented here are from two shallow cores located in North−East Greenland, the EGRIP-S7 (75.63 N, 35.98 W) and the ExNGT-B16 (73.94 N, 37.63 W) core. Both cores cover relatively recent times (EGRIP-S7: approximately 1470-2015 CE, ExNGT-B16: approximately 1880-2005 CE) and thus have a very low particle concentration. Discrete sections of these cores are presented here to illustrate the capabilities and limitations of the SPES instrument in continuous ice-core measurements.

For the determination of the error and resolution, additionally, discrete samples from different ice cores (EGRIP (Greenland), Colle Gnifetti (European Alps), EDC, and EDML (Antarctica)) were measured. Additionally, discrete measurements of the standard materials were conducted. For these measurements, we used ultra fine test dust (UFTD, NIST reference material 8632), which consists of naturally occurring irregularly shaped mineral particles and soot particles (fullerene soot (as produced), Sigma-Aldrich). A detailed description of the discrete sample preparation is given in the Supporting Information.

SPES Method. The advantages of the SPES method are that it can be integrated into a continuous flow setup and the lower size detection limit of approximately 0.2 μm. This lower detection limit is dependent on the refractive index and the sensitivity of the laser. In contrast to other techniques that give the volume size distribution, by design, the number size distribution is retrieved from the SPES measurements. Due to their strongly different scattering and extinction properties, a distinction between dielectric (nonabsorbing) and absorbing particles can be achieved.

Detection Principle. The SPES instrument detects the laser light that is transmitted and scattered by a particle passing through the laser beam in a flow cell. A quadrant photodiode registers the signal in the forward direction, which is the direction of the incident beam. The interference of the transmitted and scattered wave creates intensity fluctuations, which are proportional to the complex scattering amplitude.[24] The scattering data generated by the instrument are saved in 2D histograms (SPES-fields) with the x-axis corresponding to the logarithm of the real part of the scattering amplitude in the forward direction $\log[\mathrm{Re}\{S(0°)\}]$ and the y-axis to $\log[\mathrm{Im}\{S(0°)\}]$.

Retrieval of Size and Refractive Index. The diameter and the refractive index of a nonabsorbing particle can be determined by comparing the experimental scattering amplitude for each particle with computer simulations of spherical particles of known size and refractive index.[24] The scattering simulations used for the comparison are conducted with the open-source Amsterdam discrete dipole approximation (ADDA) code.[27] A range of scattering amplitudes is determined by simulating scattering of a plane wave with spherical particles of different combinations of sizes and refractive indices. The simulations are binned on the same grid as the experimental data, thereby creating a look-up table (LUT).

Assumptions and Implications. Some assumptions are needed for particle sizing. The most crucial is that the particles are assumed to be spherical and homogeneous in their composition. Hence, only an effective (spherical equivalent) diameter and refractive index are determined here. Note that in principle, the scattering and extinction response of nonspherical particles can be taken into account using forward scattering modeling,[28] if the particle shape is known a priori. For natural dust samples in ice cores, however, the shape and sizes are very variable and are not known for each detected particle. Moreover, the orientation of nonspherical particles relative to the incident laser beam may vary. Accordingly, here, we show results only for spherical-equivalent parameters.

The nonsphericity influences the complex scattering amplitude ($S = \mathrm{Re} + i \cdot \mathrm{Im}$) in a way that the optical thickness ($\rho = 2 \cdot \mathrm{Re}/\mathrm{Im}$) is reduced compared to spherical particles, and the spread in scattering amplitude is increased.[26,29] Here, the spherical shape is assumed in order to be left with only two unknown parameters, the diameter and the real part of the refractive index. For absorbing particles, calculating the scattering amplitude[30,31] and, thus, determining the size of the particles are not possible without assuming either the real or imaginary part of the refractive index and the morphology, which typically resembles fractal aggregates.[32] However, the estimates of refractive indices of absorbing particles vary greatly.[33,34] Additionally, the shape and morphology of carbonaceous aerosols depend strongly on their formation and aging process.[35] Therefore, we refrain from making any assumptions on the morphology and refractive index and report only the number concentration of absorbing particles, not their size.

To retrieve concentrations from the detected single particle signals, the instrument is calibrated by the manufacturer. This calibration could potentially affect the accuracy of the retrieved concentration and size distribution, as it is partly based on measurements with the standard particles.

Continuous Flow Analysis. The continuous flow analysis (CFA) pioneered in Bern[36−39] consists of a melter unit in a cold room at −20 °C and the analysis system situated in a lab at room temperature. The analysis set up consists of different fluorescence and absorption methods (wet-chemistry) and a time-of-flight ICP-MS.[40] Only the inner part of the melted ice stick is analyzed with the Bern CFA system including the SPES measurements. The ice at the ends and at breaks of the ice sticks is shaved off to decontaminate the surfaces. In a standard measurement, 4.4 m (8× 0.55 m long sticks) is melted at about 2.8 cm/min (for ice) in one run, which is achieved by

https://doi.org/10.1021/acs.est.4c07098
Environ. Sci. Technol. XXXX, XXX, XXX−XXX

reloading the ice sticks during the measurement. The system is described in detail in Kaufmann et al.[37] and Erhardt et al.[41]

In the Bern CFA setup, the SPES instrument is positioned downstream of the conductivity cell (Amber Science) and the Abakus sensor (Klotz GmbH, Germany). The meltwater is pumped through these two instruments first, before it passes the SPES with a delay from the moment of melting of approximately 100 s. The instrument in use is the EOS Classizer One, which can measure continuously in either the lower (0.2−2 μm) or the upper (2−10 μm) size range at different flow rates. In the Bern CFA system, the lower measurement range at a flow rate of 2 mL/min is typically used and described here.

The operation of the instrument in a continuous flow setup reduces the risk of contamination because only the meltwater from the inner part of the ice stick is measured. Additionally, the sample is measured immediately after melting, which reduces the likelihood of (partial) dissolution or coagulation of particles in the meltwater. Measuring in continuous mode also allows for the resolution of fast changes, such as individual mineral dust storms or wildfire events in ice cores with sufficiently high annual layer thickness. This is the case for the EGRIP site, where the annual layer thickness in the ice section of the core is about 12 cm during the Holocene.[42] Furthermore, including the SPES instrument into the CFA setup makes it possible to compare the data to other measurements thanks to the perfect alignment of the different records.

Data and Processing. The goal of the postprocessing is to put the data on a depth scale by using the melt speed and including the meta data on the break size and position. Additionally, possible contamination is reduced by excluding data around the breaks (details in Kaufmann et al.[37]). The SPES data are put on the depth scale by aligning them to the Abakus microparticle concentration data. This assumes that the seasonal cycle of dust is the dominant signal in both records, and therefore, the seasonal changes happen in parallel in the smaller and larger size range. The SPES concentration is calculated by taking the sum over each SPES-field. The time offset between the data sets of the two instruments is determined by maximizing the correlation between their z-scores. The SPES data, recorded at 1 Hz, are put on a depth scale with 1 mm resolution by taking the mean over the raw SPES-fields that fall into the respective 1 mm depth interval. At a melt speed of 2.8 cm/min ice equivalent, approximately 0.5 mm of the ice core is measured per second. Thus, each data point on the 1 mm resolution depth scale corresponds to the mean over approximately two raw SPES-fields.

Resolution. The actual resolution of the SPES concentration record depends on the instrumental noise and the dispersion of the signal due to the melting procedure and the flow through the CFA system. The rise and fall times of a step function (switch from ultrapure water to sample and back) are indicative of the resolvable signal duration. To determine the rise time, a cumulative normal distribution function is fitted to the concentration data of such a step function measurement. The rise of the signal from 10 to 90% of its final level (rise time) is determined to be approximately 10 s (Figure 1b) and is independent of the concentration. This corresponds to a depth resolution of 0.5 cm at a melt speed of 2.8 cm/min.

To investigate the effect of the dispersion on the data, we determine the upper frequency limit at which the SPES concentration data are dominated by white noise. For an upper

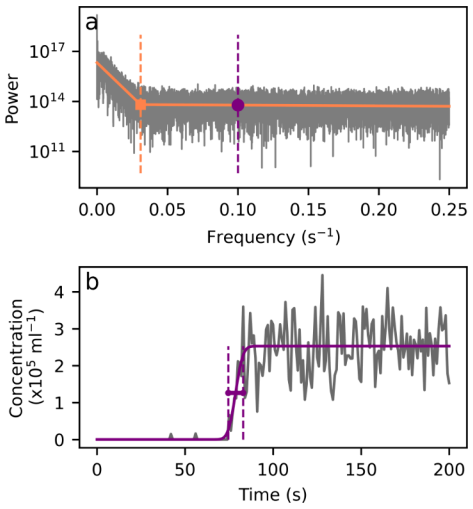

Figure 1. (a) Power spectrum of the EGRIP-S7 raw data for sections 64−84 m. The orange marker (square) indicates the frequency of the intersection of the piecewise linear function (1/32 s^{-1}). This point represents the frequency above which the signal is noise. The purple marker shows the frequency that corresponds to the rise time of the signal (1/10 s^{-1}). (b) Switch from ultrapure water to sample and fitted cumulative normal distribution (purple) with the dashed lines indicating the rise time (10th to 90th percentile) of 10 s. The orange marker being positioned at a lower frequency compared to the purple marker indicates that concentration changes in the ice core are slower than the changes the instrument could theoretically resolve (rise time).

frequency limit lower than the frequency determined from the step function, the data should not be greatly affected by smoothing in the system. By fitting a piecewise linear function to the FFT power spectrum of the raw ice-core measurement data, the upper frequency limit is determined to be 0.03 s^{-1}, corresponding to 32 s measurement time or 1.5 cm (at 2.8 cm/min melt speed). This implies that for an annual layer thickness of 12 cm, as typically found at the EGRIP site, subannual variations in the aerosol deposition can be resolved.

Uncertainties in Diameter and Refractive Index. In this study, we fit a log-normal distribution to the experimentally retrieved data and report the two fitting parameters, the median (μ) and the geometric standard deviation (σ_g). As ice-core samples are polydisperse, a certain number of scattering events needs to be registered by the instrument to get a representative size distribution of the sample. The error interval, within which the parameters of the size distribution can be determined, is thus dependent on the desired time/depth resolution and the particle concentration of the sample. For a given concentration, the error increases with increasing sampling resolution (Figure 2 and Supporting Information). We determine the relation between the uncertainty in the parameters of the size distribution and the number of measured particles experimentally using different ice-core samples spanning a wide range of concentrations. The procedure is described in detail in the Supporting Information.

RESULTS AND DISCUSSION

SPES-Field. A typical SPES-field of Holocene ice in northeastern Greenland is characterized by two distinct areas that show high concentrations of particles (denoted as modes in the following). The first one has a larger spread in the real part of the scattering amplitude in the SPES-field and is mainly

https://doi.org/10.1021/acs.est.4c07098
Environ. Sci. Technol. XXXX, XXX, XXX−XXX

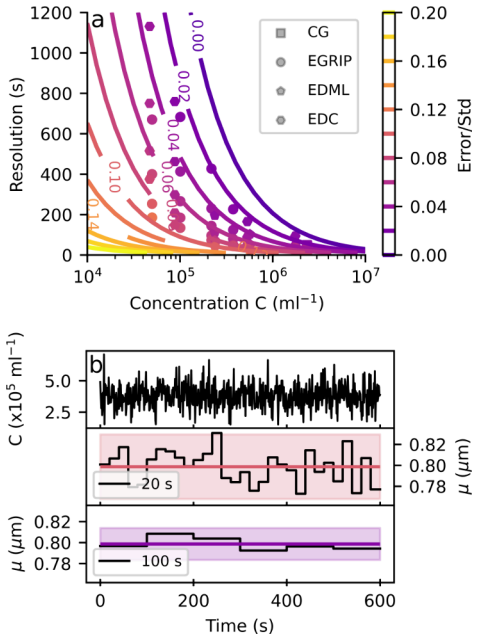

Figure 2. Error of the median diameter (μ) depends on the particle concentration (C) and the resolution (time over which the data are averaged). (a) The lines represent the error divided by the standard deviation of the diameter of the sample. The lines were obtained by fitting the data from samples from Colle Gnifetti (CG, square), EGRIP (circle), EDML (pentagon), and EDC (hexagon). (b) 600 s of a measurement of a well-mixed EGRIP sample is shown. The median diameter (μ) was determined for different resolutions (20 and 100 s) with the shaded area corresponding to the determined error (0.04 and 0.02 μm) at 95% confidence (see the Supporting Information) for the sample with a concentration of $C = 3.7 \times 10^5$ mL^{-1}.

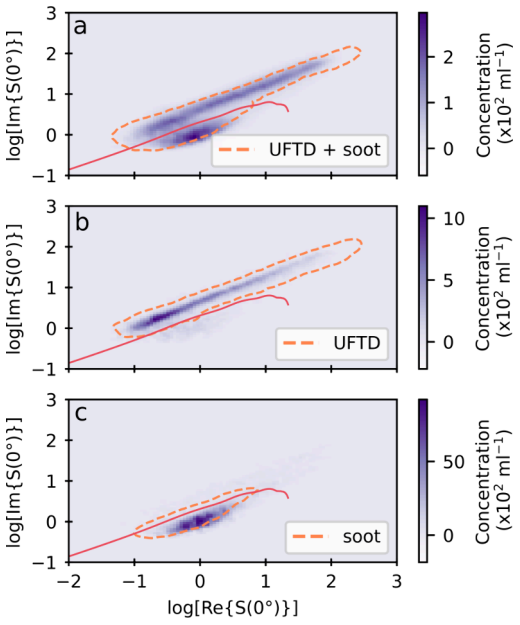

Figure 3. SPES-fields for selected ice-core data (purple, 2D histogram) and standard particles (orange, contours). (a) Mean SPES-field (70−80 m in EGRIP-S7) with a contour line of UFTD mixed with soot particles. (b) Section with high nonabsorbing particle concentration (55.12−55.85 m in EGRIP-S7 core, dust peak) with a contour line from a UFTD sample. (c) Absorbing particle peak (60.565−60.615 m in EGRIP-S7 core) with the contour line from a soot particle sample. The red line is the separating line used for the differentiation between absorbing and nonabsorbing particles.

a result from scattering of nonabsorbing (or only very weakly absorbing) particles. The second mode appears when scattering by absorbing particles takes place. This results from the distinct complex scattering amplitude of strongly absorbing and nonabsorbing particles because of their differing optical properties.

In Figure 3, average SPES-fields are depicted for the data between 70 and 80 m (Figure 3a), a dust peak (Figure 3b), and an absorbing particle peak (Figure 3c) of the EGRIP-S7 core. The orange contour lines show measurements of two standard materials: ultra fine test dust (UFTD) and soot particles. Although the properties of these standard particles do not perfectly correspond to the particles in ice cores, their SPES-fields are comparable. The small difference for absorbing particles likely results from absorbing ice-core particles not necessarily being black carbon (BC). Furthermore, the ice-core-absorbing particles are aged particles, which can have a significant effect on the refractive index and their shape and size.[35]

The dielectric and absorbing particle concentrations can be determined by taking the sum over the area of the SPES-field where the respective mode lies. To separate the respective areas, scattering simulations for particles with a refractive index of 1.9 were used (red line in Figure 3). These fall into the concentration minimum of the SPES-field between the two modes, and the refractive index of most naturally occurring mineral particles is smaller. The disadvantage of this approach is that the modes may overlap to some degree, and some of the particles can be misclassified. This overlap results from the detected particles having a range of refractive indices and shapes. An estimation of the misclassification based on standard measurements is described in the Supporting Information.

In the ice-core data presented here, the dielectric particle concentration is low and is in a range similar to the absorbing one. Therefore, the identification of absorbing particle peaks and the relative changes in concentration over longer time scales is possible solely on the basis of the scattering amplitude. For data with higher concentration differences between absorbing and nonabsorbing particles, a more sophisticated approach may be needed.

Absorbing Particles. The lower detection limit in particle diameter of the SPES only allows for the detection of particles larger than approximately 0.2 μm. This would correspond to the upper tail of the size distribution of absorbing particles in Greenland. Mori et al.[43] found a number modal diameter for BC particles in Greenland snow below 100 nm using an SP2 instrument. As the detection limit of the SPES also depends on the (complex) refractive index of the particles and because the particle sizes in SP2 and SPES are determined fundamentally different, a direct comparison is beyond the scope of this study. However, we can still expect that only the larger absorbing particles can be detected by SPES, while the majority remains hidden.

To test the hypothesis that the detected absorbing particles originate from wildfire events, we compare the data to the ammonium (NH_4^+) record for a section (corresponding to the years 1620−1640 CE) of the EGRIP-S7 core (Figure 4a). Large peaks in NH_4^+ are associated with the deposition of wildfire-derived aerosols, which can include BC.[44,45] Some of the largest peaks in the NH_4^+ record are also found in the

https://doi.org/10.1021/acs.est.4c07098
Environ. Sci. Technol. XXXX, XXX, XXX−XXX

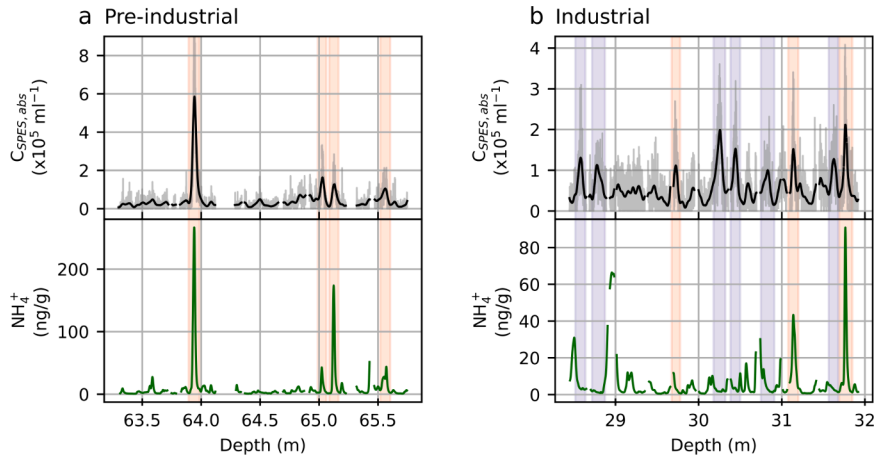

Figure 4. SPES absorbing particle concentration $C_{SPES,abs}$ (high-resolution data in gray, Gaussian smoothed data in black, $\sigma = 12$) for an ice-core section of (a) the EGRIP-S7 core in preindustrial times and (b) ExNGT-B16 in industrial times in comparison with the ammonium (NH_4^+) record. High peaks in the NH_4^+ record are associated with wildfires and are highlighted in orange. The absorbing particle peaks highlighted in purple do not coincide with the NH_4^+ peaks, suggesting their origin to be fossil fuel combustion.

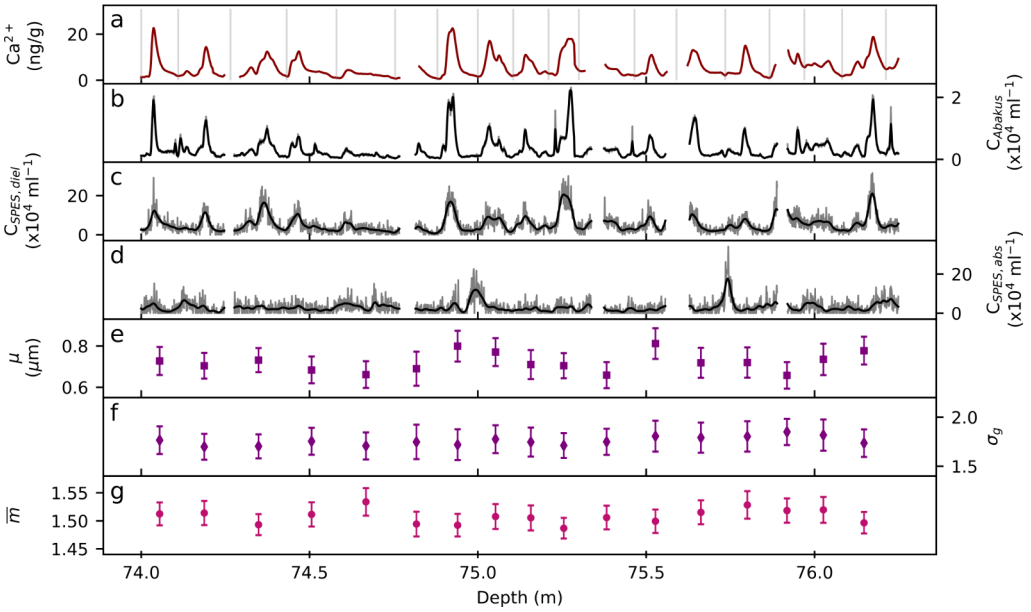

Figure 5. High-resolution ice-core data for a 2 m section of the EGRIP-S7 core. (a) The soluble dust proxy calcium (Ca^{2+}) with the gray vertical lines indicating the sections used for the calculation of the parameters in plots (e−g); (b) the Abakus particle concentration C_{Abakus} for particles larger than 1 μm; the SPES particle concentration (raw data in gray, data smoothed with a Gaussian filter ($\sigma = 6$) in black) for (c) nonabsorbing $C_{SPES,diel}$ and (d) absorbing $C_{SPES,abs}$ particles; (e) the median diameter μ and (f) the geometric standard deviation σ_g of the number size distribution; (g) the mean effective refractive index $\bar{m}$. At this resolution, no change in the size distribution parameters or the mean refractive index, considering the associated errors, is detectable.

absorbing particle concentration data, which is highlighted in orange in Figure 4a. This suggests that the absorbing particle events that can be detected with the SPES instrument in preindustrial times can be primarily attributed to wildfires. NH_4^+ peaks in the ice are not always accompanied by absorbing particle peaks or vice versa, which is explained by the fact that the fire properties that lead to NH_4^+ production may not always be conducive of the formation of absorbing particles and that the atmospheric residence times of absorbing particles and NH_4^+-bearing aerosol are different.[44]

Absorbing particles in industrial times do not always coincide with NH_4^+ peaks (Figure 4b). The ice-core section of the ExNGT-B16 record covers the period 1900−1920 CE and therefore the peak in BC concentrations found in Greenland ice.[9] The absorbing particle maxima highlighted in purple in Figure 4b do not coincide with maxima but with minima in the NH_4^+ record. Thus, they occur during the time of the year with minimal biogenic productivity (winter), suggesting that these particles are not of biogenic origin. These shifted absorbing particle peaks are likely a result of anthropogenic fossil fuel burning during the winter months.

Dielectric Particles. Overall, the SPES instrument operated in continuous mode produces results similar to those of the already established methods. The concentration of the SPES instrument and the concentration measured with the Abakus dust sensor show simultaneous changes with the calcium (Ca^{2+}) concentration, which is often taken as (soluble) dust proxy.[20] The Abakus and SPES concentration data

https://doi.org/10.1021/acs.est.4c07098
Environ. Sci. Technol. XXXX, XXX, XXX−XXX

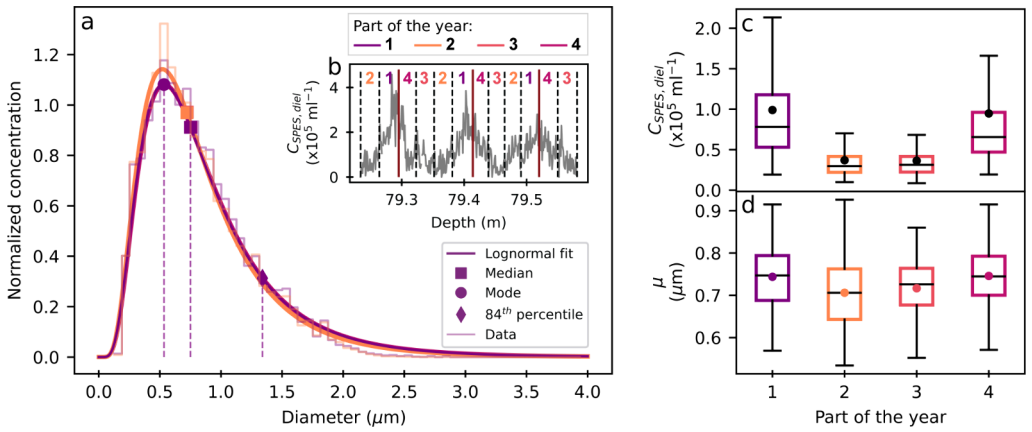

Figure 6. (a) Mean size distribution for each of (b) 4 equally long parts of an annual layer (based on the peak in Ca^{2+} corresponding to late winter to early spring) over 150 years (approximately 1625−1475 CE, 65−83 m). The size distributions of the 1st and 4th and the 2nd and 3rd parts are almost indistinguishable. Indicated are the median (square), the mode (circle), and the 84th percentile (diamond) of the fitted number size distribution to the data of the 2nd and 4th part. The boxplots show the distribution of (c) the annual dielectric particle concentration $C_{SPES,diel}$ and (d) the median diameter μ for each of the 4 parts of the year for the 150 year period.

correlate well despite their different size ranges (Figure 5b,c, Pearson correlation coefficient of 0.76 for the unfiltered data, below 60 m of the EGRIP-S7 core). This demonstrates that the seasonal changes in the dust signal in the smaller and the larger size range happen in parallel. When only considering the common size range (1−2 μm), the correlation between the two data sets is higher (0.84).

However, some significant differences between the concentration record in the common size range of Abakus and the SPES instrument exist. The high-resolution SPES concentration record is much more variable than the Abakus record. This is likely due to the much lower detection efficiency of the SPES, which only measures a small fraction of the particles in the meltwater stream. Even though this is corrected for by the instrument software, this results in lower counting statistics and a higher noise in the data.

Potential inaccuracies in this estimation of the concentration based on the single particle signals are also one possible cause for the SPES concentrations being approximately four times larger than those from the Abakus. The other possible cause for this is the lack of a good size calibration of the Abakus instrument employed in these measurements. For natural, nonspherical particles found in the ice, uncalibrated Abakus size distribution measurements are skewed toward larger particles.[46] Thus, the concentration in the size range between 1 and 2 μm is underestimated in our Abakus measurements. Considering this, the retrieved absolute concentration values should be considered with caution. However, relative concentration changes detected with SPES are not affected by a potential overestimation of the concentration.

Besides the high-resolution particle concentration measurements, the SPES instrument offers the opportunity to investigate the effective diameter and refractive index distributions. The median diameter of the fitted size distribution, the geometric standard deviation, and the mean refractive index are shown for each annual concentration maximum in a 2 m section of the EGRIP-S7 core, with the associated errors in Figure 5e−g. No changes in these parameters are detected within their errors due to the noise in the SPES raw data (see Figure 2). This implies that for an investigation of the seasonality, a stacking of several years (or peaks) is necessary to obtain statistically significant results for samples of low concentrations.

To investigate possible seasonal differences in median diameter, every annual layer below 65 m (approximately 1625 CE) of the EGRIP-S7 core was divided into four equal parts. The annual layer boundary was set to the annual concentration maximum in the Ca^{2+} record, which is observed in late winter to early spring (January−March) at the EGRIP site in recent years.[47] A mean SPES-field over each part of every year was calculated and normalized. A 150 year mean SPES-field for each of the four parts was determined from the normalized SPES-fields. The log-normal size distribution was fit to each part (Figure 6a). The instrumental uncertainty (according to the determination described in the Supporting Information) for this data is negligible, and only the standard deviations of the parameters of the fit are reported in the following.

The median diameter retrieved from the fit for the first and fourth part of the year (annual concentration maximum) is (0.75 ± 0.01) μm, and the geometric standard deviation is found to be 1.79 ± 0.02. For the second and third part of the year (annual concentration minimum), a median diameter of (0.72 ± 0.01) μm and a geometric standard deviation of 1.76 ± 0.02 and 1.77 ± 0.02, respectively, were determined from the fit. Thus, the median diameter is different between the annual dust minimum and the maximum, while the geometric standard deviation does not differ within the fitting uncertainty.

In order to illustrate the spread in concentration and median diameter over the 150 year period, the log-normal size distribution was also fit to each annual quarterly SPES-field. This is depicted in boxplots for the concentration and median diameter for the four parts of the year in Figure 6c,d. It appears that the median diameter is the largest during the part of the year with the highest dust input (spring) and the lowest during the minimum in annual dust concentration. Therefore, a seasonal signal appears not only in the concentration but also in the median diameter of the size distribution.

The origin of dust in Greenland ice cores varies seasonally,[48] which could potentially affect the size distribution of the particles. Transport time and deposition mechanisms also modulate the size distribution and concentration,[49] as larger

https://doi.org/10.1021/acs.est.4c07098
Environ. Sci. Technol. XXXX, XXX, XXX−XXX

particles are more efficiently removed from the air column and dry and wet depositions depend differently on particle size.[50] Additionally, changes in source region mobilization affect the particle concentration.[51] This is illustrated by the annual dust concentration maximum observed in Greenland ice cores during late winter/early spring[47] concurring with dust storms in Asia.[52] Therefore, seasonal variability in precipitation during transport and to the ice sheet, as well as in source region contribution, could result in the higher median diameter during the annual dust concentration maximum in the investigated period from 1475 to 1625 CE. As there are several potential mechanisms that could result in the observed differences in size distribution, dedicated research is needed to confidently attribute them.

To comprehensively understand these seasonal differences, it is essential to interpret them in the context of changing atmospheric circulation, source region mobilization, and depositional mechanisms. Future applications of the instrument may include investigating long-term climatic and seasonal variations in particle concentration, effective diameter, and refractive index. Integrating the SPES instrument into a CFA setup enhances the ability to measure these physical properties of particles preserved in ice cores. The information gained from the addition of the SPES could help disentangle the processes, leading to variations in these parameters.

■ ASSOCIATED CONTENT

Supporting Information

The Supporting Information is available free of charge at https://pubs.acs.org/doi/10.1021/acs.est.4c07098.

Description of the discrete sampling procedure, the fit used to obtain the size distribution parameters, the error calculation, and additional figures for the error of the geometric standard deviation and the mean refractive index, as well as additional information on the separation of absorbing and nonabsorbing particles based on the scattering amplitude (PDF)

■ AUTHOR INFORMATION

Corresponding Author

Chantal Zeppenfeld − *Climate and Environmental Physics, Physics Institute, and Oeschger Centre for Climate Change Research, University of Bern, Bern 3012, Switzerland;* orcid.org/0000-0002-6340-5836; Email: chantal.zeppenfeld@unibe.ch

Authors

Tobias Erhardt − *Climate and Environmental Physics, Physics Institute, and Oeschger Centre for Climate Change Research, University of Bern, Bern 3012, Switzerland; Institute of Geosciences and Frankfurt Isotope and Element Research Center (FIERCE), Goethe University Frankfurt, Frankfurt am Main 60438, Germany*

Camilla Marie Jensen − *Climate and Environmental Physics, Physics Institute, and Oeschger Centre for Climate Change Research, University of Bern, Bern 3012, Switzerland*

Hubertus Fischer − *Climate and Environmental Physics, Physics Institute, and Oeschger Centre for Climate Change Research, University of Bern, Bern 3012, Switzerland*

Complete contact information is available at: https://pubs.acs.org/10.1021/acs.est.4c07098

Notes

The authors declare no competing financial interest.

■ ACKNOWLEDGMENTS

The long-term financial support of ice-core research at the University of Bern by the Swiss National Science Foundation (grant nos. 200020_172506 & 200020B_20038 (iCEP1&2) and 20FI21_164190 (EGRIP)) is gratefully acknowledged. EGRIP is directed and organized by the Centre for Ice and Climate at the Niels Bohr Institute, University of Copenhagen. It is supported by funding agencies and institutions in Denmark (A. P. Møller Foundation, University of Copenhagen), USA (US National Science Foundation, Office of Polar Programs), Germany (Alfred Wegener Institute, Helmholtz Centre for Polar and Marine Research), Japan (National Institute of Polar Research and Arctic Challenge for Sustainability), Norway (University of Bergen and Trond Mohn Foundation), Switzerland (Swiss National Science Foundation), France (French Polar Institute Paul-Emile Victor, Institute for Geosciences and Environmental research), Canada (University of Manitoba), and China (Chinese Academy of Sciences and Beijing Normal University). We also want to express our gratitude to the people who facilitated and took part in both the ice-core drilling and processing as well as the CFA melting campaign. Furthermore, we would like to thank EOS for their personalized support.

■ REFERENCES

(1) Harrison, S. P.; Kohfeld, K. E.; Roelandt, C.; Claquin, T. The Role of Dust in Climate Changes Today, at the Last Glacial Maximum and in the Future. *Earth Sci. Rev.* **2001**, *54* (1−3), 43−80.

(2) Svensson, A.; Biscaye, P. E.; Grousset, F. E. Characterization of Late Glacial Continental Dust in the Greenland Ice Core Project Ice Core. *Journal of Geophysical Research: Atmospheres* **2000**, *105* (D4), 4637−4656.

(3) Bory, A. J.; Biscaye, P. E.; Grousset, F. E. Two Distinct Seasonal Asian Source Regions for Mineral Dust Deposited in Greenland (NorthGRIP). *Geophys. Res. Lett.* **2003**, *30* (4), 1−4.

(4) Vancuren, R. A.; Cahill, T.; Burkhart, J.; Barnes, D.; Zhao, Y.; Perry, K.; Cliff, S.; Mcconnell, J. Aerosols and Their Sources at Summit Greenland e First Results of Continuous Size- and Time-Resolved Sampling. *Atmos. Environ.* **2012**, *52*, 82−97.

(5) Han, C.; Do Hur, S.; Han, Y.; Lee, K.; Hong, S.; Erhardt, T.; Fischer, H.; Svensson, A. M.; Steffensen, J. P.; Vallelonga, P. High-Resolution Isotopic Evidence for a Potential Saharan Provenance of Greenland Glacial Dust. *Sci. Rep.* **2018**, *8* (1), No. 15582.

(6) Újvári, G.; Klötzli, U.; Stevens, T.; Svensson, A.; Ludwig, P.; Vennemann, T.; Gier, S.; Horschinegg, M.; Palcsu, L.; Hippler, D.; Kovács, J.; Di Biagio, C.; Formenti, P. Greenland Ice Core Record of Last Glacial Dust Sources and Atmospheric Circulation. *Journal of Geophysical Research: Atmospheres* **2022**, *127* (15), No. e2022JD036597.

(7) Ro, S.; Park, J.; Yoo, H.; Han, C.; Lee, A.; Lee, Y.; Kim, M.; Han, Y.; Svensson, A.; Shin, J.; Ro, C. U.; Hong, S. Millennial-Scale Variability of Greenland Dust Provenance during the Last Glacial Maximum as Determined by Single Particle Analysis. *Sci. Rep.* **2024**, *14* (1), 2040.

(8) Li, Y.; Song, Y.; Li, X.; Kaskaoutis, D. G.; Gholami, H.; Li, Y. Disentangling Variations of Dust Concentration in Greenland Ice Cores over the Last Glaciation: An Overview of Current Knowledge and New Initiative. *Earth Sci. Rev.* **2023**, *242*, No. 104451.

(9) McConnell, J. R.; Edwards, R.; Kok, G. L.; Flanner, M. G.; Zender, C. S.; Saltzman, E. S.; Banta, J. R.; Pasteris, D. R.; Carter, M. M.; Kahl, J. D. W. 20th-Century Industrial Black Carbon Emissions Altered Arctic Climate Forcing. *Science (1979)* **2007**, *317* (5843), 1381−1384.

(10) Hegg, D. A.; Warren, S. G.; Grenfell, T. C.; Doherty, S. J.; Larson, T. V.; Clarke, A. D. Source Attribution of Black Carbon in Arctic Snow. *Environ. Sci. Technol.* **2009**, *43* (11), 4016−4021.
(11) Zennaro, P.; Kehrwald, N.; McConnell, J. R.; Schüpbach, S.; Maselli, O. J.; Marlon, J.; Vallelonga, P.; Leuenberger, D.; Zangrando, R.; Spolaor, A.; Borrotti, M.; Barbaro, E.; Gambaro, A.; Barbante, C. Fire in Ice: Two Millennia of Boreal Forest Fire History from the Greenland NEEM Ice Core. *Climate of the Past* **2014**, *10* (5), 1905−1924.
(12) Martin, J. H. Glacial-interglacial CO2 Change: The Iron Hypothesis. *Paleoceanography* **1990**, *5* (1), 1−13.
(13) Bristow, C. S.; Hudson-Edwards, K. A.; Chappell, A. Fertilizing the Amazon and Equatorial Atlantic with West African Dust. *Geophys. Res. Lett.* **2010**, *37* (14), L14807.
(14) Mahowald, N. Aerosol Indirect Effect on Biogeochemical Cycles and Climate. *Science (1979)* **2011**, *334* (6057), 794−796.
(15) Sokolik, I. N.; Winker, D. M.; Bergametti, G.; Gillette, D. A.; Carmichael, Y. J.; Kaufman, Y. J.; Gomes, L.; Schuetz, L.; Penner, J. E. Introduction to Special Section: Outstanding Problems in Quantifying the Radiative Impacts of Mineral Dust. *Journal of Geophysical Research Atmospheres* **2001**, *106* (16), 18015−18027.
(16) Haywood, J.; Boucher, O. Estimates of the Direct and Indirect Radiative Forcing Due to Tropospheric Aerosols: A Review. *Reviews of Geophysics* **2000**, *38* (4), 513−543.
(17) Lohmann, U.; Feichter, J. Atmospheric Chemistry and Physics Global Indirect Aerosol Effects: A Review. *Atmos. Chem. Phys.* **2005**, *5*, 715−737.
(18) Kok, J. F.; Storelvmo, T.; Karydis, V. A.; Adebiyi, A. A.; Mahowald, N. M.; Evan, A. T.; He, C.; Leung, D. M. Mineral Dust Aerosol Impacts on Global Climate and Climate Change. *Nature Reviews Earth & Environment* **2023**, *4* (2), 71−86.
(19) Albani, S.; Mahowald, N. M. Paleodust Insights into Dust Impacts on Climate. *J. Clim* **2019**, *32* (22), 7897−7913.
(20) Ruth, U.; Barbante, C.; Bigler, M.; Delmonte, B.; Fischer, H.; Gabrielli, P.; Gaspari, V.; Kaufmann, P.; Lambert, F.; Maggi, V.; Marino, F.; Petit, J. R.; Udisti, R.; Wagenbach, D.; Wegner, A.; Wolff, E. W. Proxies and Measurement Techniques for Mineral Dust in Antarctic Ice Cores. *Environ. Sci. Technol.* **2008**, *42* (15), 5675−5681.
(21) Drab, E.; Gaudichet, A.; Jaffrezo, J. L.; Colin, J. L. Mineral Particles Content in Recent Snow at Summit (Greenland). *Atmos. Environ.* **2002**, *36* (34), 5365−5376.
(22) Nagatsuka, N.; Goto-Azuma, K.; Tsushima, A.; Fujita, K.; Matoba, S.; Onuma, Y.; Dallmayr, R.; Kadota, M.; Hirabayashi, M.; Ogata, J.; Ogawa-Tsukagawa, Y.; Kitamura, K.; Minowa, M.; Komuro, Y.; Motoyama, H.; Aoki, T. Variations in Mineralogy of Dust in an Ice Core Obtained from Northwestern Greenland over the Past 100 Years. *Climate of the Past* **2021**, *17* (3), 1341−1362.
(23) Steffensen, J. P. The Size Distribution of Microparticles from Selected Segments of the Greenland Ice Core Project Ice Core Representing Different Climatic Periods. *J. Geophys Res. Oceans* **1997**, *102* (C12), 26755−26763.
(24) Potenza, M. A. C.; Sanvito, T.; Pullia, A. Measuring the Complex Field Scattered by Single Submicron Particles. *AIP Adv.* **2015**, *5* (11), 117222.
(25) Potenza, M. A. C.; Cremonesi, L.; Delmonte, B.; Sanvito, T.; Paroli, B.; Pullia, A.; Baccolo, G.; Maggi, V. Single-Particle Extinction and Scattering Method Allows for Detection and Characterization of Aggregates of Aeolian Dust Grains in Ice Cores. *ACS Earth Space Chem.* **2017**, *1* (5), 261−269.
(26) Potenza, M. A. C.; Albani, S.; Delmonte, B.; Villa, S.; Sanvito, T.; Paroli, B.; Pullia, A.; Baccolo, G.; Mahowald, N.; Maggi, V. Shape and Size Constraints on Dust Optical Properties from the Dome C Ice Core, Antarctica. *Sci. Rep* **2016**, *6* (1), 28162.
(27) Yurkin, M. A.; Hoekstra, A. G. The Discrete-Dipole-Approximation Code ADDA: Capabilities and Known Limitations. *J. Quant Spectrosc Radiat Transf* **2011**, *112* (13), 2234−2247.
(28) Cremonesi, L.; Minnai, C.; Ferri, F.; Parola, A.; Paroli, B.; Sanvito, T.; Potenza, M. A. C. Light Extinction and Scattering from Aggregates Composed of Submicron Particles. *J. Nanopart. Res.* **2020**, *22* (11), 1−17.
(29) Villa, S.; Sanvito, T.; Paroli, B.; Pullia, A.; Delmonte, B.; Potenza, M. A. C. Measuring Shape and Size of Micrometric Particles from the Analysis of the Forward Scattered Field. *J. Appl. Phys.* **2016**, *119* (22), No. 224901.
(30) Sorensen, C. M. Light Scattering by Fractal Aggregates: A Review. *Aerosol Sci. Technol.* **2001**, *35* (2), 648−687.
(31) Potenza, M. A. C.; Cremonesi, L. An Overview of the Optical Characterization of Free Microparticles and Their Radiative Properties. *J. Quant Spectrosc Radiat Transf* **2023**, *311*, No. 108773.
(32) Xiong, C.; Friedlander, S. K. Morphological Properties of Atmospheric Aerosol Aggregates. *Proc. Natl. Acad. Sci. U. S. A.* **2001**, *98* (21), 11851−11856.
(33) Bond, T. C.; Bergstrom, R. W. Light Absorption by Carbonaceous Particles: An Investigative Review. *Aerosol Sci. Technol.* **2006**, *40* (1), 27−67.
(34) Alexander, D. T. L.; Crozier, P. A.; Anderson, J. R. Brown Carbon Spheres in East Asian Outflow and Their Optical Properties. *Science* **2008**, *321* (5890), 833−836.
(35) China, S.; Mazzoleni, C.; Gorkowski, K.; Aiken, A. C.; Dubey, M. K. Morphology and Mixing State of Individual Freshly Emitted Wildfire Carbonaceous Particles. *Nat. Commun.* **2013**, *4* (1), 1−7.
(36) Röthlisberger, R.; Bigler, M.; Hutterli, M.; Sommer, S.; Stauffer, B.; Junghans, H. G.; Wagenbach, D. Technique for Continuous High-Resolution Analysis of Trace Substances in Firn and Ice Cores. *Environ. Sci. Technol.* **2000**, *34* (2), 338−342.
(37) Kaufmann, P. R.; Federer, U.; Hutterli, M. A.; Bigler, M.; Schüpbach, S.; Ruth, U.; Schmitt, J.; Stocker, T. F. An Improved Continuous Flow Analysis System for High-Resolution Field Measurements on Ice Cores. *Environ. Sci. Technol.* **2008**, *42* (21), 8044−8050.
(38) Sigg, A.; Fuhrer, K.; Anklln, M.; Staffelbach, T.; Zurmühle, D. A Continuous Analysis Technique for Trace Species in Ice Cores. *Environ. Sci. Technol.* **1994**, *28* (2), 204−209.
(39) Bigler, M.; Svensson, A.; Kettner, E.; Vallelonga, P.; Nielsen, M. E.; Steffensen, J. P. Optimization of High-Resolution Continuous Flow Analysis for Transient Climate Signals in Ice Cores. *Environ. Sci. Technol.* **2011**, *45* (10), 4483−4489.
(40) Erhardt, T.; Jensen, C. M.; Borovinskaya, O.; Fischer, H. Single Particle Characterization and Total Elemental Concentration Measurements in Polar Ice Using Continuous Flow Analysis-Inductively Coupled Plasma Time-of-Flight Mass Spectrometry. *Environ. Sci. Technol.* **2019**, *53* (22), 13275−13283.
(41) Erhardt, T.; Jensen, C. M.; Adolphi, F.; Kjaer, H. A.; Dallmayr, R.; Twarloh, B.; Behrens, M.; Hirabayashi, M.; Fukuda, K.; Ogata, J.; Burgay, F.; Scoto, F.; Crotti, I.; Spagnesi, A.; Maffezzoli, N.; Segato, D.; Paleari, C.; Mekhaldi, F.; Muscheler, R.; Darfeuil, S.; Fischer, H. High-Resolution Aerosol Data from the Top 3.8 Kyr of the East Greenland Ice Coring Project (EGRIP) Ice Core. *Earth Syst. Sci. Data* **2023**, *15*, 5079−5091.
(42) Mojtabavi, S.; Wilhelms, F.; Cook, E.; Davies, S. M.; Sinnl, G.; Skov Jensen, M.; Dahl-Jensen, D.; Svensson, A.; Vinther, B. M.; Kipfstuhl, S.; Jones, G.; Karlsson, N. B.; Faria, S. H.; Gkinis, V.; Kjær, H. A.; Erhardt, T.; Berben, S. M. P.; Nisancioglu, K. H.; Koldtoft, I.; Rasmussen, S. O. A First Chronology for the East Greenland Ice-Core Project (EGRIP) over the Holocene and Last Glacial Termination. *Clim. Past Discuss.* **2020**, *16* (6), 2359−2380.
(43) Mori, T.; Goto-Azuma, K.; Kondo, Y.; Ogawa-Tsukagawa, Y.; Miura, K.; Hirabayashi, M.; Oshima, N.; Koike, M.; Kupiainen, K.; Moteki, N.; Ohata, S.; Sinha, P. R.; Sugiura, K.; Aoki, T.; Schneebeli, M.; Steffen, K.; Sato, A.; Tsushima, A.; Makarov, V.; Omiya, S.; Sugimoto, A.; Takano, S.; Nagatsuka, N. Black Carbon and Inorganic Aerosols in Arctic Snowpack. *Journal of Geophysical Research: Atmospheres* **2019**, *124* (23), 13325−13356.
(44) Legrand, M.; McConnell, J.; Fischer, H.; Wolff, E. W.; Preunkert, S.; Arienzo, M.; Chellman, N.; Leuenberger, D.; Maselli, O.; Place, P.; Sigl, M.; Schüpbach, S.; Flannigan, M. Boreal Fire

https://doi.org/10.1021/acs.est.4c07098
Environ. Sci. Technol. XXXX, XXX, XXX−XXX

Records in Northern Hemisphere Ice Cores: A Review. *Clim. Past* **2016**, *12*, 2033−2059.
(45) Fischer, H.; Schüpbach, S.; Gfeller, G.; Bigler, M.; Röthlisberger, R.; Erhardt, T.; Stocker, T. F.; Mulvaney, R.; Wolff, E. W. Millennial Changes in North American Wildfire and Soil Activity over the Last Glacial Cycle. *Nat. Geosci* **2015**, *8* (9), 723−727.
(46) Simonsen, M. F.; Cremonesi, L.; Baccolo, G.; Bosch, S.; Delmonte, B.; Erhardt, T.; Kjær, H. A.; Potenza, M.; Svensson, A.; Vallelonga, P. Particle Shape Accounts for Instrumental Discrepancy in Ice Core Dust Size Distributions. *Climate of the Past* **2018**, *14* (5), 601−608.
(47) Kjær, H. A.; Zens, P.; Black, S.; Lund, K. H.; Svensson, A.; Vallelonga, P. Canadian Forest Fires, Icelandic Volcanoes and Increased Local Dust Observed in Six Shallow Greenland Firn Cores. *Climate of the Past* **2022**, *18* (10), 2211−2230.
(48) Bory, A. J. M.; Biscaye, P. E.; Svensson, A.; Grousset, F. E. Seasonal Variability in the Origin of Recent Atmospheric Mineral Dust at NorthGRIP, Greenland. *Earth Planet Sci. Lett.* **2002**, *196* (3−4), 123−134.
(49) Ruth, U.; Wagenbach, D.; Steffensen, J. P.; Bigler, M. Continuous Record of Microparticle Concentration and Size Distribution in the Central Greenland NGRIP Ice Core during the Last Glacial Period. *Journal of Geophysical Research D: Atmospheres* **2003**, *108* (3), 1−12.
(50) Seinfeld, J. H.; Pandis, S. N. *Atmospheric Chemistry and Physics: From Air Pollution to Climate Change*, 2nd ed.; John Wiley & Sons, Ltd, 2006.
(51) Fuhrer, K.; Wolff, E. W.; Johnsen, S. J. Timescales for Dust Variability in the Greenland Ice Core Project (GRIP) Ice Core in the Last 100,000 Years. *J. Geophys. Res.: Atmos.* **1999**, *104* (D24), 31043−31052.
(52) Sun, J.; Zhang, M.; Liu, T. Spatial and Temporal Characteristics of Dust Storms in China and Its Surrounding Regions, 1960−1999: Relations to Source Area and Climate. *Journal of Geophysical Research: Atmospheres* **2001**, *106* (D10), 10325−10333.

https://doi.org/10.1021/acs.est.4c07098
Environ. Sci. Technol. XXXX, XXX, XXX−XXX